Remote Sens. **2014**, *6*, 1327-1346; doi:10.3390/rs6021327

OPEN ACCESS

remote sensing

ISSN 2072-4292

www.mdpi.com/journal/remotesensing

Article

Absolute Calibration of Optical Satellite Sensors Using Libya 4 Pseudo Invariant Calibration Site

Nischal Mishra [1,2,*], Dennis Helder [1], Amit Angal [3], Jason Choi [4] and Xiaoxiong Xiong [5]

[1] Department of Electrical Engineering & Computer Science, South Dakota State University (SDSU), Brookings, SD 57007, USA; E-Mail: Dennis.helder@sdstate.edu

[2] Image Processing Lab, Department of Electrical Engineering & Computer Science, South Dakota State University, Daktronics Engineering Hall, Room 315, P.O. BOX 2219, SDSU, Brookings, SD 57007, USA

[3] Science Systems and Applications Inc., 10210 Greenbelt Road, Lanham, MD 20706, USA; E-Mail: Amit.Angal@ssaihq.com

[4] Sigma Space Corporation, Lanham, MD 20706, USA; E-Mail: taeyoung.choi@sigmaspace.com

[5] NASA Goddard Space Flight Center (GSFC), Greenbelt, MD 20771, USA; E-Mail: Xiaoxiong.Xiong.1@gsfc.nasa.gov

* Author to whom correspondence should be addressed; E-Mail: nischal.mishra@sdstate.edu; Tel.: +1-605-688-4372; Fax: +1-605-688-7969.

Received: 15 December 2013; in revised form: 23 January 2014 / Accepted: 26 January 2014 / Published: 12 February 2014

Abstract: The objective of this paper is to report the improvements in an empirical absolute calibration model developed at South Dakota State University using Libya 4 (+28.55°, +23.39°) pseudo invariant calibration site (PICS). The approach was based on use of the Terra MODIS as the radiometer to develop an absolute calibration model for the spectral channels covered by this instrument from visible to shortwave infrared. Earth Observing One (EO-1) Hyperion, with a spectral resolution of 10 nm, was used to extend the model to cover visible and near-infrared regions. A simple Bidirectional Reflectance Distribution function (BRDF) model was generated using Terra Moderate Resolution Imaging Spectroradiometer (MODIS) observations over Libya 4 and the resulting model was validated with nadir data acquired from satellite sensors such as Aqua MODIS and Landsat 7 (L7) Enhanced Thematic Mapper (ETM+). The improvements in the absolute calibration model to account for the BRDF due to off-nadir measurements and annual variations in the atmosphere are summarized. BRDF models due to off-nadir viewing angles have been derived using the measurements from EO-1 Hyperion. In addition to L7

ETM+, measurements from other sensors such as Aqua MODIS, UK-2 Disaster Monitoring Constellation (DMC), ENVISAT Medium Resolution Imaging Spectrometer (MERIS) and Operational Land Imager (OLI) onboard Landsat 8 (L8), which was launched in February 2013, were employed to validate the model. These satellite sensors differ in terms of the width of their spectral bandpasses, overpass time, off-nadir-viewing capabilities, spatial resolution and temporal revisit time, *etc.* The results demonstrate that the proposed empirical calibration model has accuracy of the order of 3% with an uncertainty of about 2% for the sensors used in the study.

Keywords: radiometric calibration; absolute calibration; PICS; BRDF; Landsat; MODIS

1. Introduction

Absolute calibration is a process that converts the voltage recorded by a satellite sensor or digitized counts to an absolute radiance unit. It is known that the calibration of a satellite-based sensor may be subjected to changes due to phenomena such as outgassing, variation in the filter transmittance and spectral response, and slow deterioration of the electronic system, *etc.* Ongoing absolute calibration is necessary to characterize and assess the performance throughout a sensor's lifetime from prelaunch phase through on-orbit operations so that radiometrically accurate image data can be continuously provided to the user community. Over the years, different techniques have been used to perform both the prelaunch laboratory calibration and the post-launch on-orbit calibration. During prelaunch calibration, a series of elements are calibrated and characterized. These include the optical sensors themselves, the optical path components, and onboard calibrators such as lamps, blackbodies and reflectance panels. The calibrations are generally devised to be SI traceable and are a means to validate mission requirement performance. Post-launch calibration includes different techniques such as measurement of on-board calibrators, vicarious calibration, cross calibration between satellite sensors, use of stellar and lunar sources, *etc.*

One of the least expensive and increasingly popular methods of on-orbit calibration has been the use of pseudo invariant calibration sites (PICS). The advantages of using these spatially uniform sites are their stable spectral characteristics over time, high reflectance, and minimal atmospheric effect on upward radiance. As a result, these sites have been used extensively by researchers to monitor the multi-temporal and multi-angular stability of satellite sensors using time series analysis and cross-calibration [1–6]. However, PICS alone have the potential to be used for absolute calibration. The scenario is similar to prelaunch calibration where a sensor views a calibration panel illuminated uniformly with a source in the laboratory; conversely, while in orbit, the sensor views PICS illuminated by the sun. The approach is very low cost since the primary expenditure is the effort required to collect routine imagery of the PICS. Sites have been identified for which it is easy to schedule image acquisitions without impacting the normal operational data collection practices of the satellite system. This approach also provides an excellent mechanism for inter-comparison of sensors.

Despite the obvious advantages, very little research has been done to explore the capabilities and challenges of developing an absolute calibration model using these PICS as compared to primary

usage for basic trending and cross-calibration. Govaerts *et al.* have done the initial work in developing an absolute calibration model using PICS with geostationary satellites [7,8]. In these papers, the solar irradiance was used as a forcing function along with a bidirectional surface reflectance model based on a three-parameter bare soil approach. Atmospheric modeling was done using 6S as the radiative transfer code with reliance on Total Ozone Mapping Spectrometer (TOMS) data for aerosol estimation. Results indicate accuracies in the 3% range for the red and near-infrared bands, with uncertainties approaching 6%. Since then, improvements have been made in his model with the use of an advanced radiative transfer model that accounts for polarization, improves the surface reflectance characterization and provides for the use of a non-spherical aerosol model. The results presented by Govaerts in 2012 showed that, over Libya 4, it is possible to achieve a mean accuracy of 3% using observations from PARASOL, MERIS, AATSR, Aqua MODIS and VEGETATION 2 [9].

Bhatt *et al.* developed a desert daily exoatmospheric radiance model (DERM) based on a well-calibrated (reference) geostationary Earth orbit (GEO) satellite visible sensor [10]. This can be used to transfer the calibration to a (non-calibrated target) GEO sensor located at the same equatorial longitude location. In the study, the GEO-specific PICS are first inspected with Aqua MODIS and the GEO reference calibration was based on the GEO/Aqua-MODIS ray-matched radiance intercalibration technique. The daily exoatmospheric radiance was constructed using all the operational years of the reference GEO. The PICS-specific hyperspectral data from the Scanning Imaging Absorption SpectroMeter for Atmosphere Chartography (SCIAMACHY) instrument onboard the European environmental (ENVISAT) satellite was used to account for the spectral band differences between the reference and target GEO satellites. Their results showed that reference Meteostat-9 DERM and ray-matched calibration consistency was within 0.4% and 1.9% for Meteostat-8 and Meteostat-7, respectively, using Libya 4 PICS.

Helder *et al.* presented the concept of an empirical absolute calibration model using a well-calibrated sensor in 2012 [11]. They developed an absolute calibration model using the Libya 4 test site, where Terra MODIS was used as the calibrated radiometer, and hyperspectral observations from EO-1 Hyperion were used for the spectral signature. A simple BRDF model was derived using Terra MODIS observations. The model was validated with L7 ETM+, which showed that the agreement between the model and satellite-measured TOA reflectance was 6% RMSE with a random uncertainty around 2%. The objective of this paper is to expand this work by Helder *et al.* in order to develop an empirical absolute calibration model using PICS that can be used for the estimate of absolute calibration of any sensor with a viewing zenith angle of up to 20 degrees. This paper is organized into 4 sections. The introduction section provides a brief review of absolute calibration and some of the earlier work done using PICS to develop an absolute calibration model, the second section discusses the Libya 4 PICS and the sensors used for the current study, and the third section describes the methodologies used to develop absolute calibration methods and some of the validation results. A summary section concludes the paper.

2. Libya 4 Pics and Satellite Observations

Radiometric calibration trending using invariant sites on the Earth's surface has been used for more than a decade [1–6,12–14]. These sites are popularly known in the calibration validation fraternity as

PICS. Helder *et al.* have developed an algorithm to identify and categorize the potential PICS, along with their most spatially and temporally stable region, using Landsat 5 images from 1984 through 2011 [15]. The algorithm calculates the temporal stability of the potential PICS by ratioing the temporal standard deviation by the temporal mean. Results from this work supported the use of the Committee on Earth Observation Satellites (CEOS) reference sites and indicated that stability in the range of 1%–3% was possible. A suite of sites has been developed and endorsed by CEOS and includes locations in Libya, Algeria, Niger and Mauritania (can be currently viewed at http://calval.cr.usgs.gov/sites_catalog_ceos_sites.php#CEOS) [16]. A net result is that the site commonly known as Libya 4 has been shown to be one of the most stable of these sites and hence is widely used. It is located in the Landsat WRS-2 path 181 and row 40. This site is made up of sand dunes with no vegetation, exhibits reasonable spatial, spectral, and temporal uniformity, and nominally has minimal to no cloud cover. Analysis of ETM+ observations over Libya 4 has shown that linear drift of the sensor on the order of 0.2% per year could be measured over its 13+ years of operation [17].

Figure 1. Temporal uncertainties of various Saharan PICS.

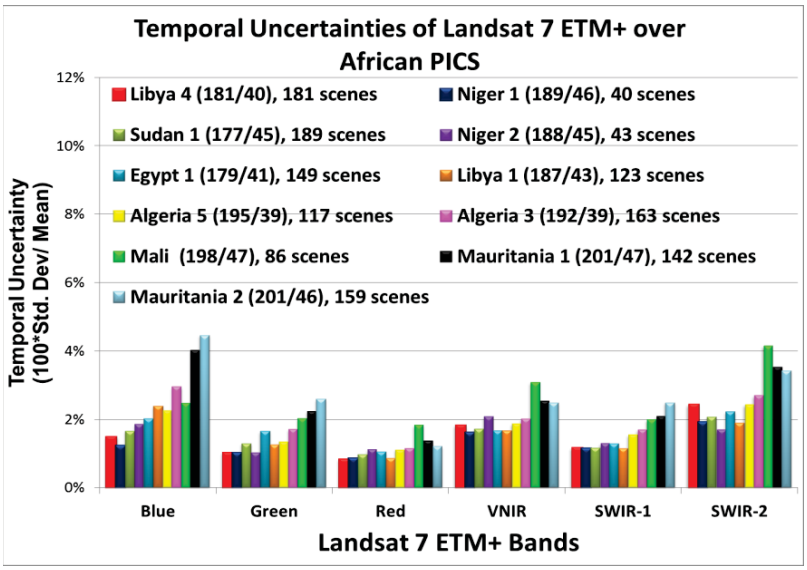

PICS-based calibration is only good as long as the sites being used continue to exhibit a reasonable spatial, temporal and spectral stability. In order to study the stability of several of the African PICS endorsed by CEOS, ETM+ observations spanning from 2000 to 2013 were trended as a function of time. The exact regions of interest (ROI) have been described in various articles [1,15]. Figure 1 shows the temporal uncertainties in terms of the coefficient of variation (standard deviation divided by the mean), of these PICS for all the solar reflective ETM+ bands along with the number of cloud-free images used in the study. An attempt has been made to rank these uncertainties from the lowest to the highest for each band. It can be seen that Libya 4 and Niger sites rank among top PICS based on lower uncertainties (<2%) in each of the spectral bands from visible to shortwave infrared (SWIR) as measured in terms of top of atmosphere reflectance. Libya 4 has been selected for this work since this site is regularly imaged by other satellites including Aqua, Terra, DMC, Rapid Eye, *etc.* for monitoring the sensors' temporal stabilities. Studies done with EO-1 Hyperion over Libya 4 suggest that a sensor

can be calibrated to better than 1% accuracy with the implementation of a BRDF model in a transparent atmosphere [11]. Further studies done using Hyperion over Libya 4 have shown this site to be spectrally stable where Spectral Angle Mapper (SAM) angles are less than 1.6 degrees and average deviations are less than 5% reflectance level based on reference spectrum in 2004 within ETM+ RSR Full-Width at Half-Maximum (FWHM) ranges [18].

Table 1 provides, for several satellites used in this current study, the nominal center wavelengths of their spectral channels and the numbers of observations over Libya 4. L7 ETM+ and L8 OLI images were processed using the Landsat Image Assessment (IAS) system. Landsat 8 was launched in February 2013, thus only six cloud-free acquisitions were available at the time of this work. Terra and Aqua MODIS Collection 6 datasets were provided by the MODIS Characterization Support Team, with ENVISAT MERIS values obtained from the ESA DIMITRI database. UK-2 images were provided by the DMCii Team UK and have green, red and near-infrared (NIR) channels, as shown in Table 1. The image data for all sensors were then converted into physical units of TOA reflectance using the standard techniques and equations applicable for each sensor. It should be noted that this work was initially done for the absolute calibration of Landsat [11]. Therefore, for the sensors under examination here, only the spectral bands that have spectral overlap with Landsat have been chosen. The satellites used provide a good sample of narrowband and wideband sensors in different spectral regions, different revisit cycles, and overpass times in order to best validate the absolute calibration model. Figure 2 shows the Terra MODIS image and ETM+ image over Libya 4 acquired on 29 April 2003. The footprint of ETM+ is about 187 km by 187 km and Terra MODIS is about 2,030 km by 1,354 km, which is significantly greater in comparison to L7 ETM+. The red rectangle in a MODIS image (upper left) shows the full size of ETM+ image within MODIS swath. In order to present the ROI clearly, the Terra MODIS image shown in Figure 2 (bottom left) has been cropped from its full size.

Figure 2. Terra MODIS and ETM+ image over Libya 4. Upper two images are the full-sized MODIS and ETM+ images. The red rectangle in the bottom images marks the chosen region of interest (ROI) with latitude (min and max): 28.45, 28.64, longitude (min and max): 23.29, 23.4 and the size is about 19.75 km by 22.25 km. The spatial resolution of Terra MODIS (**Left**) is 250 m and that of Landsat (**Right**) is 30 m.

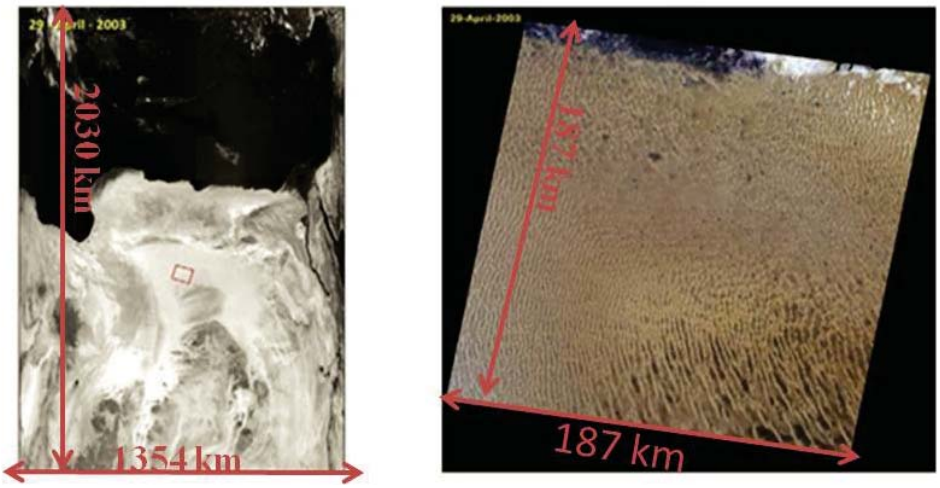

Figure 2. *Cont.*

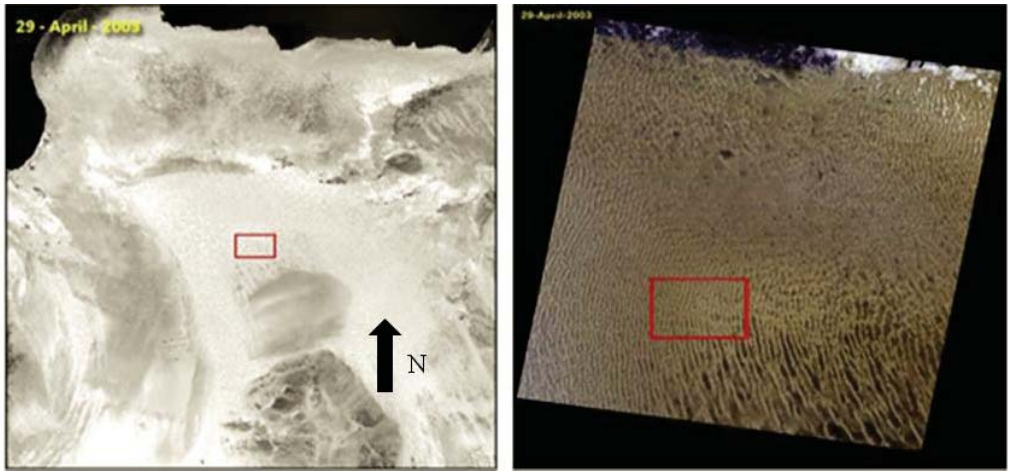

Table 1. Satellite sensors, spectral bands and number of observations used in the current study.

Satellites	Number of Images	Spectral Bandwidths (nm)					
		Blue	Green	Red	NIR	SWIR-1	SWIR-2
Landset 7 ETM+	181	450–515	525–605	630–690	775–900	1,550–1,750	2,090–2,350
Landset 8 OLI	6	450–515	525–600	630–680	845–885	1,560–1,660	2,100–2,300
Terra MODIS	155	459–479	545–565	620–670	841–876	1,628–1,652	2,105–2,155
AQUA MODIS	190	459–479	545–565	620–670	841–876	1,628–1,652	2,105–2,155
MERIS	112	435–450	552–567	657–672	852–877		
UK-2 DMC	61		520–600	630–690	770–900		

3. Development of Empirical Absolute Calibration Model Using Libya 4 Pics

3.1. Scaling the Hyperion to Terra MODIS

Helder *et al.* have described an approach to derive the absolute calibration model using a well-calibrated sensor in 2012 [5]. The method used Terra MODIS as the reference, and the Hyperion hyperspectral sensor as the source for the spectral profile. By using MODIS as a source for absolute calibration, a normalization factor can be calculated to scale the Hyperion spectrum so that, when integrated over the MODIS spectral bandpass, it will produce the comparable TOA reflectance of Terra MODIS. The scale factor was calculated using five available pairs of MODIS/Hyperion scenes that were collected essentially simultaneously (within 30 min) with nadir-viewing angles (±5°) and an essentially constant solar zenith angle of 30 ± 5°. The gain factors that were obtained on each date and for each MODIS band (listed in order of increasing wavelength) are shown in Table 2. All average gain values agree to within ±3%, indicating good consistency between the two sensors at all wavelengths with uncertainties (standard deviation/mean) in each measurement of 2% or less. Statistical analysis indicated that the mean values could be clustered into three groups: band 7, bands 2, 3 and 6 in one cluster, with bands 1 and 4 in another cluster (significance level, $\alpha = 0.05$). The final step for calculating the scale factor was to linearly interpolate the values in Table 1 in those spectral ranges covered by the MODIS bands.

Table 2. Gain factors derived from five simultaneous overpasses of Libya 4 from Terra MODIS and Hyperion [11].

MODIS Bands	4 July 2004	6 September 2004	22 September 2004	25 September 2005	24 June 2006	15 September 2007	Average	STD
3(459–479 nm)	1.025	0.992	1.001	0.998	0.973	0.979	0.995	1.82%
4(545–565 nm)	1.029	1.006	1.008	1.009	1.000	1.000	1.009	1.05%
1(620–670 nm)	1.024	1.010	1.007	1.013	1.003	1.001	1.010	0.83%
2(841–876 nm)	0.993	0.990	0.978	0.998	0.973	0.983	0.984	0.81%
6(1,628–1,652 nm)	0.996	1.001	0.991	0.999	0.977	0.984	0.992	0.95%
7(2,105–2,155 nm)	0.986	0.974	0.960	0.966	0.952	0.954	0.965	1.32%

3.2. BRDF Model

Various models from the literature have classified BRDF as physical (based on first principle), semi-empirical or empirical models. A physics-based BRDF model—taking, for instance, sand—is based on the complete characterization of physical characteristics of the sand such as its composition, irregular particle shape, refractive index, surface roughness, spectral reflectance, *etc.* Widely used semi-empirical models such as the Ross-Li model [19], Roujean model [20], and Snyder model [21] are kernel driven, whereas BRDF is modeled as a weighted sum of volume scattering, geometric scattering and isotropic terms. These kernels are derived from approximations to physical BRDF models, so that they retain physical meaning. A study done over bright desert targets with the use of the Snyder model on Polarization and Anisotropy of Reflectance for Atmospheric Sciences Couples with Observations from a Lidar (PARASOL) data has suggested that bidirectional effects are limited to reflectance variations of about 15% [22].

In this approach, the empirical BRDF model is derived using the apparent trends between TOA reflectance *versus* solar zenith angle and viewing zenith angle. While the obvious disadvantage of using the empirical model is the need for the large number of data samples to build the statistical model, it will be shown in the coming sections that the model works reasonably well for the sensors if the sensor viewing angles are restricted to within ±20 degrees of nadir.

3.2.1. BRDF Model for Solar Zenith Angle

An empirical BRDF model to account for the varying solar zenith angle was derived using nadir-looking Terra MODIS observations. Approximately 160 observations of Libya 4 at scene center (nadir ±7.5°) acquired over 3,000 days were plotted as a function of solar zenith angle (SZA), as shown in Figure 3. The plot shows good coverage of solar zenith angles ranging from 16 degrees to 56 degrees. Although the surface reflectance model such as the Ross-Li or Snyder model, is more complicated and rigorous than a linear fit, it was found that a model like the Ross-Li [16], which has a cubic term, did not provide a statistically significant improvement over a linear model. Thus, a simple linear model was fitted to the data to provide a first-order BRDF correction factor based upon solar zenith angle. Figure 2 shows an example of the linear fit for MODIS Band 2 (NIR). A similar model was generated for the six solar reflective bands of Terra MODIS. The slope of the linear term of these

six bands was then plotted *versus* center wavelength, as shown in the Figure 4. The plot shows that the BRDF changes as a function of wavelength, with the SWIR channel exhibiting a greater impact on BRDF. Figure 4 also shows that these coefficients, derived using linear fit, could be further modeled using a two-piece exponential fit with very low value of residual error, supporting the use of this model.

Figure 3. Simple linear BRDF correction model for Libya 4 based on solar zenith angle.

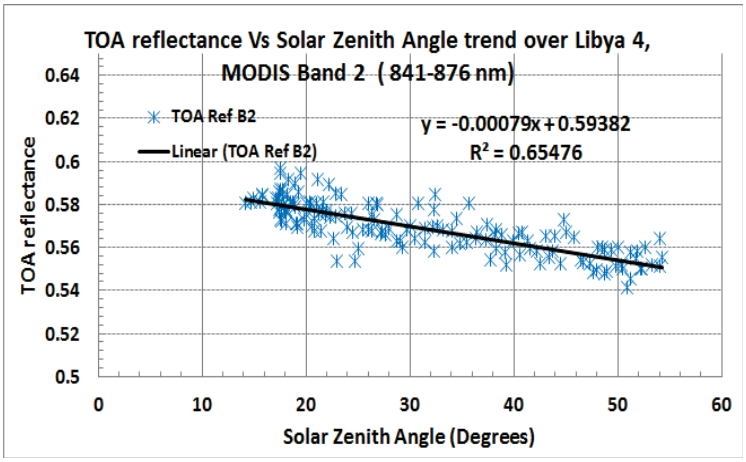

Figure 4. Exponential model to express BRDF due to solar zenith angle as a function of wavelength for Libya 4.

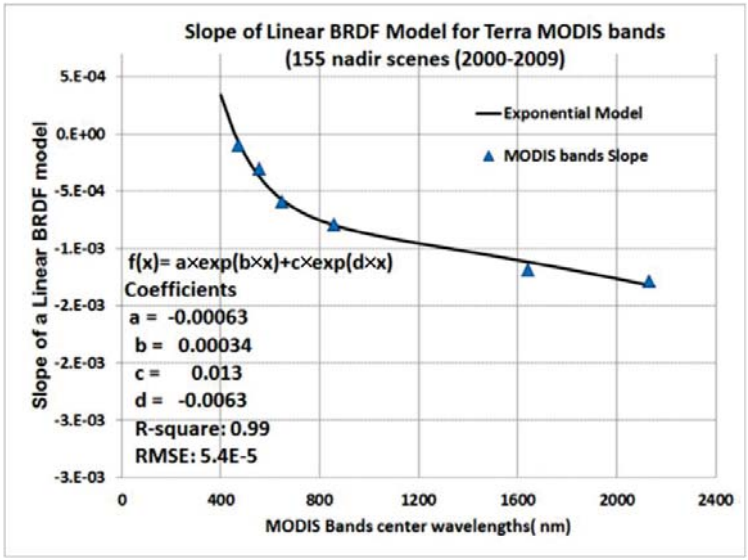

3.2.2. BRDF Model for Viewing Zenith Angle

BRDF, due to varying viewing zenith angle (VZA), was modeled in a similar way. In this case, spectrally cleaner (high transmittance and reflectance), each bandwidth of approximately 10 nm, they were used to build the model. Figure 5 shows TOA reflectance plotted as a function of viewing zenith angle for the 1,628 nm Hyperion channel, where the atmosphere is nearly transparent. It can be also seen from the plot that the VZA for Hyperion is confined to ±18 degrees. As stated previously, the equations for surface BRDF models can be complex, such as the Ross-Li model [19], but a simple second order polynomial was

found to be an adequate estimate for BRDF correction for this desert site (a higher order fit was not statistically justifiable). The procedure was repeated for eight different Hyperion channels centered on a spectral region where there is minimal atmospheric effect. When the slope of the first order and second order term was plotted as a function of wavelength, it was noticed that the slope of the first order terms was essentially constant. However it turned out that the coefficient of the second order term could be modeled as a two-exponential function of wavelength with very low residual error as shown in Figure 6.

Figure 5. Quadratic model to express BRDF due to view zenith angle as a function of wavelength for Libya 4.

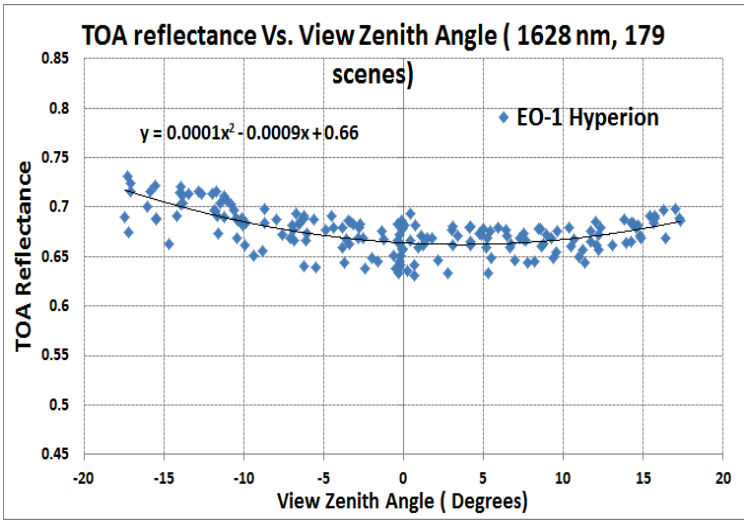

Figure 6. Exponential model to express BRDF due to view zenith angle as a function of wavelength for Libya 4.

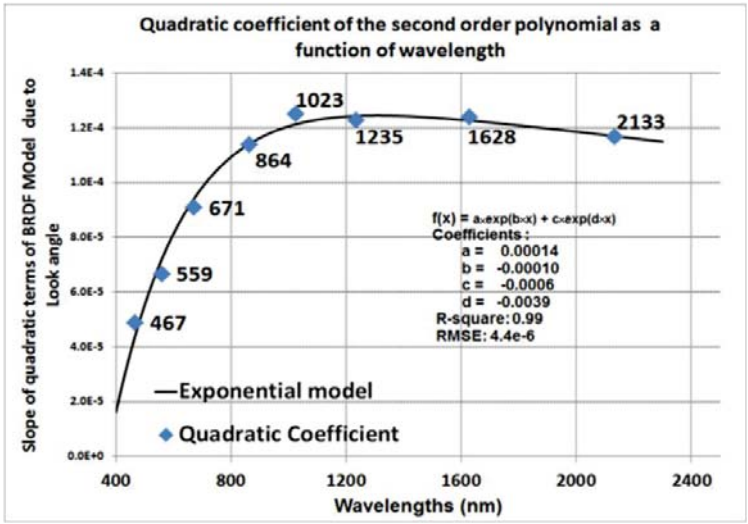

The net result is an empirical BRDF model for solar zenith and viewing zenith angle that parameterizes changes in angular reflectance as an exponential function of wavelength. It was also observed that the solar azimuth and the solar zenith angles were highly correlated because of the

limited samples of the satellite data with respect to these angles as the orbital conditions were fairly fixed. Thus, only the BRDF changes due to solar zenith angle need to be addressed.

3.3. Development of Atmospheric Model

At this point in the development of the model, all major surface parameters have been accounted for. However, it must be emphasized that in this semi-empirical approach, these have been derived as observed from top-of-atmosphere. The next step is to extend the model to include atmospheric correction. In general, a typical atmospheric model is achieved using a full up radiative transfer model using tools such as MODTRAN [23], 6S [24], *etc.*, where parameters such as aerosol optical depth, columnar water vapor, different gaseous composition are provided to the model to provide an estimate of the upward radiance scattered from the atmosphere, diffuse radiances, upwelling and downwelling transmittances, *etc.* In the empirical approach presented here, the model is based on sensor data observed from the top-of-atmosphere.

Figure 7. Magnitude and phase of cosine function used to model the atmospheric effects as a periodic sinusoid for Libya 4.

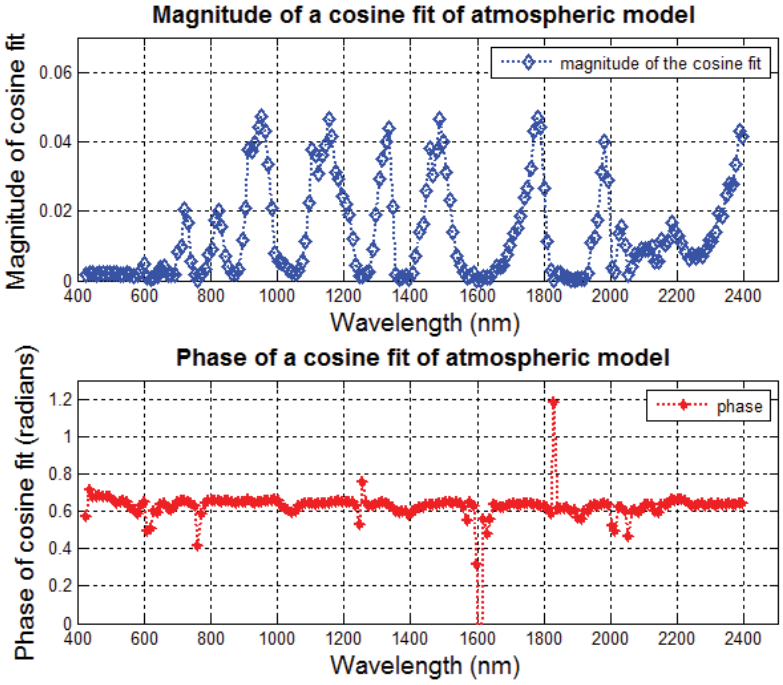

After applying the model to long time series of Landsat data, it was observed that residual seasonal variations exist. For example, TOA reflectance was still slightly higher in the summer months than in the winter months even after surface effects had been removed. This suggests small changes in the atmosphere likely due to seasonal changes in aerosol patterns and molecular absorption. Even though quite small in magnitude, they could be identified through Fourier analysis of the residuals and a simple cosine function was derived and added to the model to account for these seasonal patterns. The value of the magnitude and phase of this function is shown in Figure 7 as calculated for each Hyperion wavelength. Not surprisingly, the phase was essentially constant and the period was 365.2 days.

Figures 8 and 9 show the Hyperion TOA reflectance profile derived using 108 cloud-free images over Libya 4 and standard deviation in TOA reflectance from 2004 to 2010 plotted as a function of center wavelength, respectively. It can be seen from these plot that the apparent TOA reflectance is very low or close to zero at wavelengths where atmospheric absorption occurs and the variability is also high at these wavelengths. On comparing these plots with the magnitude plot in Figure 7, it can be seen that the magnitude as calculated by the atmospheric model is higher around the major atmospheric absorption wavelengths; the higher the magnitude of the absorption, the higher is the amplitude of the atmospheric model. On the other hand, when statistical tests indicated that the slope of the phase response is zero, *i.e.*, the phase of the model is fairly constant and, for simplicity, an average phase of 0.63 was used for calculation purposes.

Figure 8. EO-1 Hyperion TOA reflectance profile.

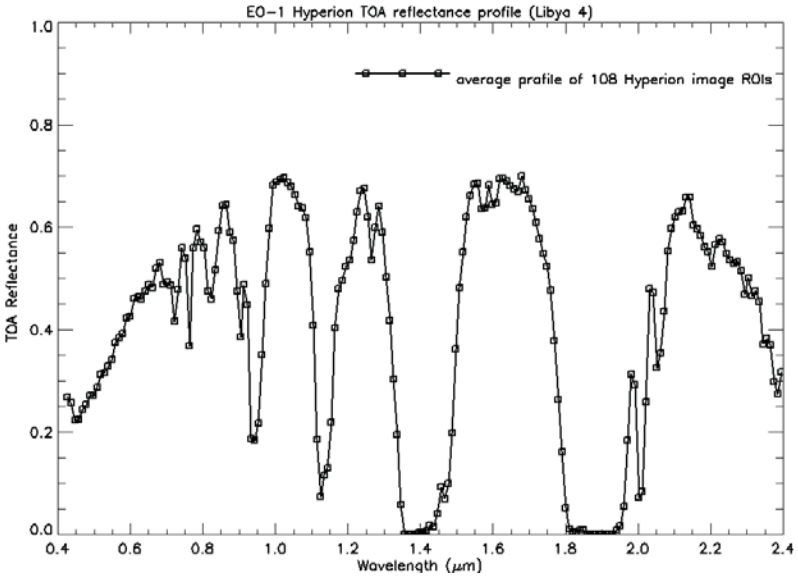

Figure 9. Standard deviation of 108 EO-1 Hyperion TOA reflectance profile.

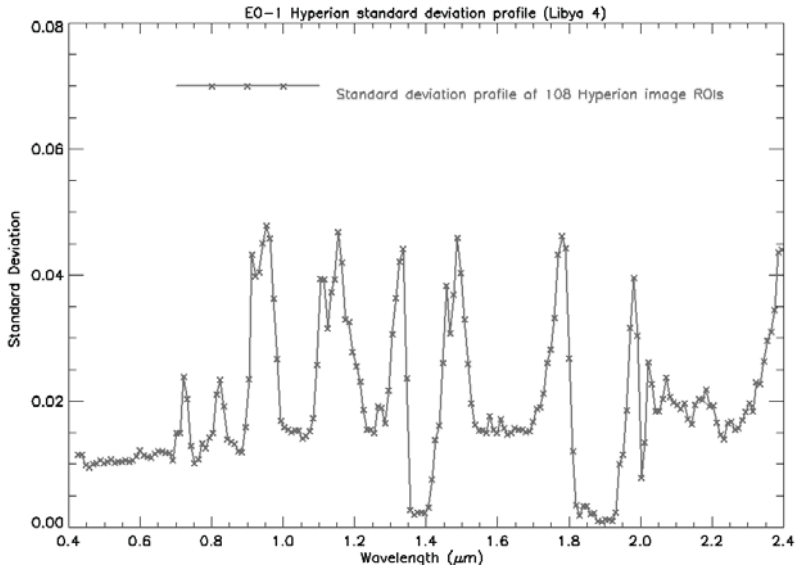

Thus the resulting simple model is

$$\rho_{Libya\,4}(\lambda, SZA, VZA) = \frac{K(\lambda) \times \rho_h(\lambda) \times f_A(t)}{(1 - (SZA - 30°) \times m_1(\lambda) - VZA(\lambda) \times m_2(\lambda) - (VZA)^2 \times m_3(\lambda))} \quad (1)$$

where ρ represents the TOA spectral reflectance for the Libya 4 PICS using Hyperion, $K(\lambda)$ is the scaling factor to place the Hyperion spectra $\rho_h(\lambda)$, on the MODIS-calibrated scale described in Section 3.1, $f_A(t)$ represents the atmospheric model which is a function of time of year as described in Section 3.3, $m_1(\lambda)$, $m_2(\lambda)$ and $m_3(\lambda)$ represent the coefficients needed for SZA and VZA correction as described in Section 3.1. The BDRF model has been scaled to a 30-degree solar zenith angle. This model is a modification differing from that presented by Helder *et al.* [5] as it has a functional form of the BRDF model to include off-nadir-viewing angles in the range of ±20° and a simple atmospheric model.

Figure 10. Terra MODIS observations of Libya 4 (blue asterisk) and model predictions (black circles).

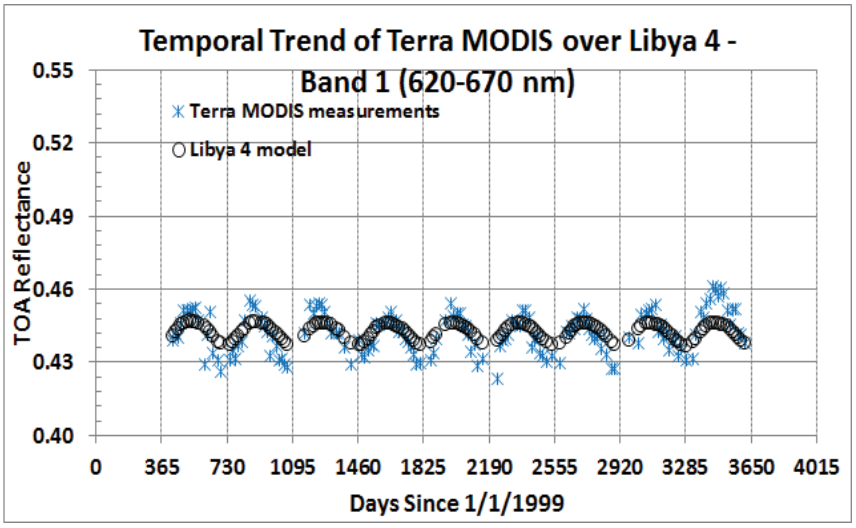

Since the model is based on Terra MODIS, the first step test of the efficacy of the model was to implement it on the Terra MODIS measurements themselves. For convenience, blue asterisks have been used for satellite observation and black circles for the Libya 4 model. The output of the model has been presented in two ways: as systematic offset (bias) calculated as root mean squared error (RMSE) between model predictions and satellite measurements, and as random uncertainties calculated as the standard deviation of the offset between model predictions and satellite measurements. It should also be noted that the percentage difference is calculated as model-predicted values minus the satellite values divided by the model. Figure 10 illustrates the application of this model to Terra MODIS red band (band 1 for MODIS and band 3 for Landsat) data collected over Libya 4, while Figure 11 shows the percentage difference between the model predictions and the MODIS measurements. The bias between the model and the measurements is 1.39% with a standard deviation of 1.3%. Table 3 shows the summarized results for different solar reflective MODIS bands obtained using the same approach. The RMSE, or bias between the model and MODIS, is under 2% in all bands and is well within the combined uncertainties of MODIS and Hyperion upon which the

model was based. The inclusion of the atmospheric model improves the standard deviation presented in the article by Helder *et al.* [11], especially at the longer wavelengths, by about 0.4%. The scatter in the residues (labeled "STD of residues" in Table 3) is an indication of how much of the model is yet to be explained. Atmospheric, higher order BRDF effects and also small random deviations in instrument response could all be contributing factors. In this case, the level of instability of the atmosphere over the Libya 4 site, at least with respect to the MODIS spectral bandpasses, is evident with differences between model prediction and satellite measurements is essentially between 1% and 2%.

Figure 11. Percentage differences between Terra MODIS observations and model predictions.

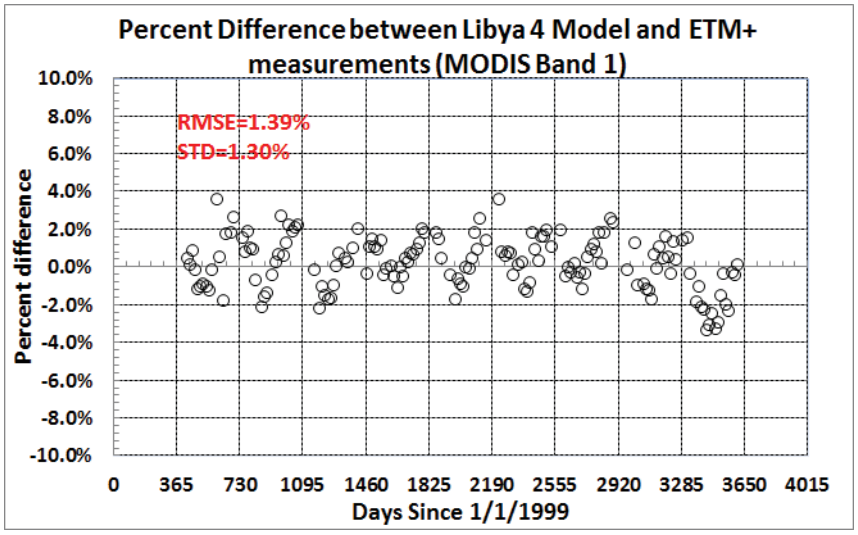

Table 3. Systematic offsets and random uncertainties between absolute calibration model predictions and Terra MODIS observations.

MODIS Bands	Root Mean Square Error (RMSE)	Standard Dev. of Residues (STD)
3 (459–479 nm)	1.20%	1.15%
4(545–565 nm)	1.13%	1.13%
1 (620–670 nm)	1.39%	1.15%
2 (841–876 nm)	1.42%	1.17%
6 (1628–1652 nm)	1.04%	0.95%
7 (2105–2155 nm)	1.81%	1.80%

3.4. Validation of the Model Using Satellite Measurements

As mentioned earlier, the measurements from different sets of well-calibrated satellite sensors were used to validate the model. These instruments include Terra and Aqua MODIS, L7 ETM+ and L8 OLI, ENVISAT MERIS and UK-2 DMC and it is important to note that these sensors were calibrated independently of Terra MODIS. Results for the red band of several of these sensors will be shown and the results for all the bands will be summarized in this section. For MERIS, the red band located at 0.657–0.672 μm has been chosen to show as a representative.

A comparison can be made between the Libya 4 model prediction and at-sensor reflectance derived from ETM+ measurements as shown in Figure 12 where the circles show the absolute calibration

prediction and the asterisks show ETM+ measurements for band 3 ("red" band). It should be noted that the radiometric calibration of the L7 ETM+ was updated in March 2013 and a detailed description of the process has been presented by Barsi *et al.* [14]. The results presented in this section are based on the updated calibration. Figure 13 shows the percentage difference between the model predictions and satellite measurements, which is on the order of 1.1% RMSE. Thus, these results are well within the specified calibration uncertainties associated with these sensors (5% for Landsat, 2% for MODIS). It is interesting to compare the results shown in Figures 7–10. The amount of bias between the model and the measurements is similar for both instruments. Also, in both cases, there is a random variability (standard deviation of differences between model prediction and satellite measurements) of about 1% attributable primarily to atmospheric differences and site spectral behavior.

Figure 12. ETM+ observations of Libya 4 (blue asterisk) and model predictions (black circles).

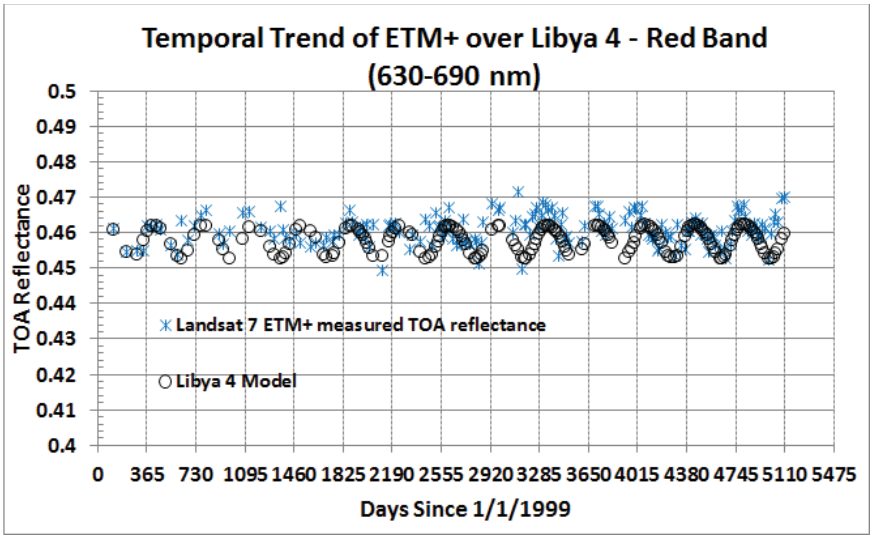

Figure 13. Percentage differences between ETM+ observations and model prediction.

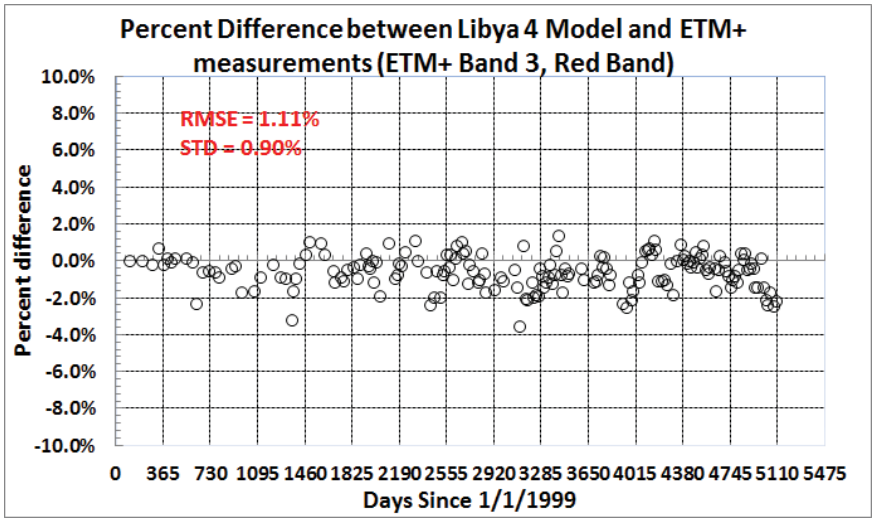

Figure 14 illustrates the application of this model to UK2 DMC data that was collected over Libya 4 from 2009 to 2012. The viewing angle for these datasets ranged from nadir to 18 degrees. Figure 15 shows the percent difference between the model predictions and the UK2 DMC measurements. The bias between the model and the measurements is 1.54% with a standard deviation of 1.54%. Note that while spectral bandpasses for ETM+ and DMC are similar, atmospheric scattering caused by non-nadir-viewing geometries may have not have been adequately explained by the model. This may have caused the standard deviation to be slightly higher than ETM+.

Figure 14. DMC observations of Libya 4 (blue asterisk) and model predictions (black circles).

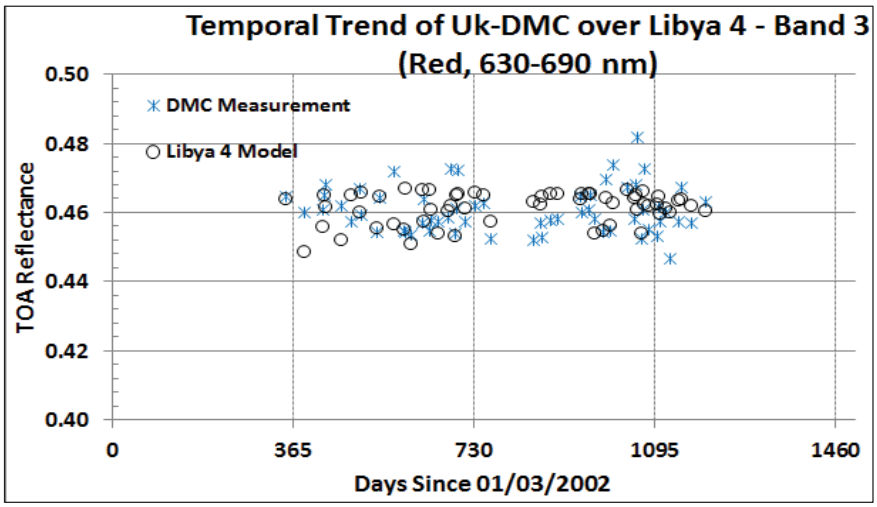

Figure 15. Percent difference between DMC observations and model prediction.

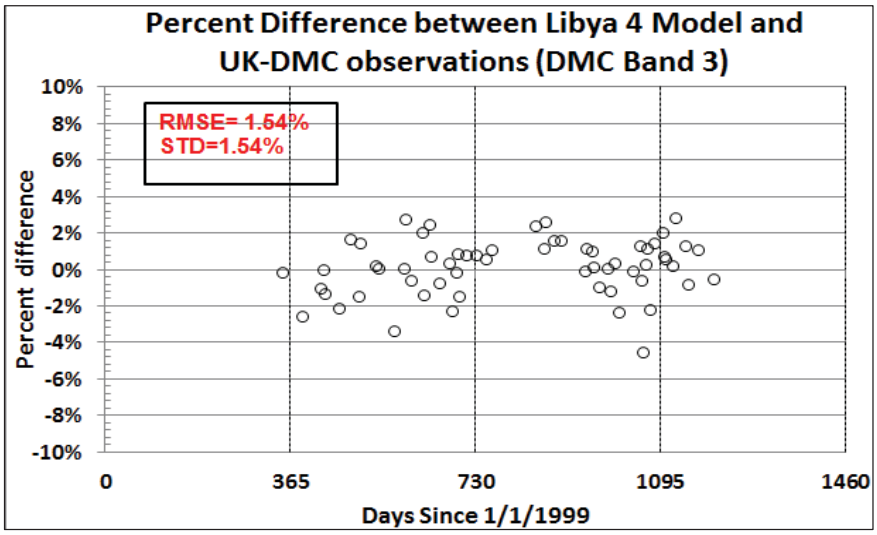

A similar approach is applied to all the sensors introduced earlier through the visible to SWIR bands and the results are summarized in Figures 16 and 17. The RMSE or bias between the model and satellite-measured values, which are illustrated in Figure 16, shows that in general, the systematic, as well as random uncertainty, is within 3%. The offset between model predictions and L7 ETM+ SWIR

and MERIS green channels approaches 4%. This offset between the model and satellite-measured values are likely based on real differences in the calibration of not only ETM+, MERIS and Terra MODIS but also Hyperion calibration uncertainties. Figure 17 shows the estimates of random variability in the model. In general, these uncertainties are within 2%. The Terra MODIS and MERIS spectral bandpasses are narrower and avoid the molecular features more than Landsat and DMC instruments, and are therefore less affected by changes in the atmosphere. In the case of MERIS and DMC, these uncertainties are probably increased due to the increased path length scattering due to non-nadir acquisitions which is not adequately explained by the empirical model.

Figure 16. Estimate of the systematic offset between satellite observations and model prediction.

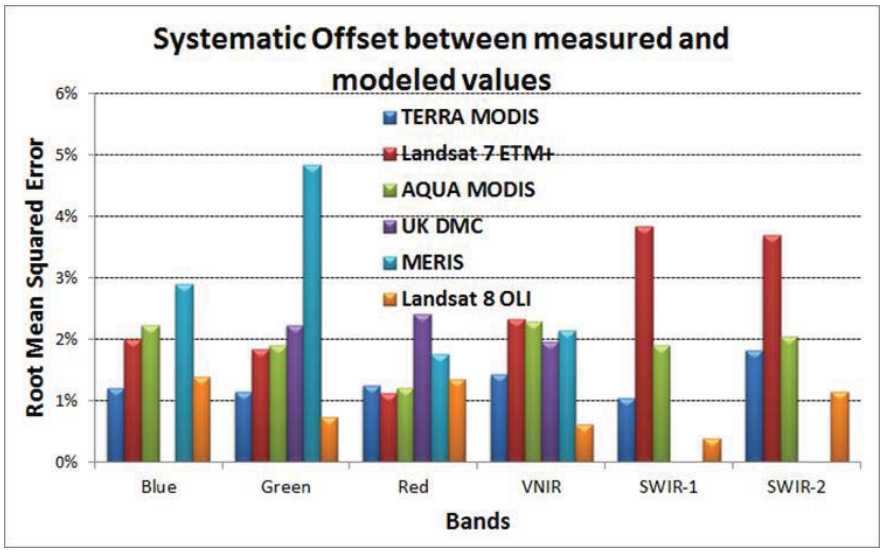

Figure 17. Estimate of the systematic offset between satellite observations and model prediction.

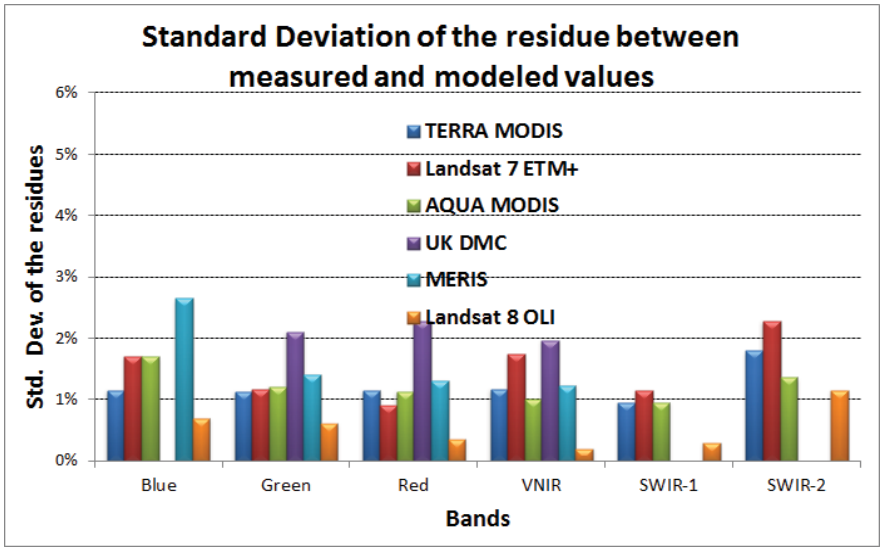

It should also be noted that the stated absolute calibration accuracy of Terra MODIS is about 2% and that of Hyperion is about 4%. The combined uncertainty (assumed uncorrelated) of these instruments is 4.5%. Thus, in all the cases, differences predicted by the model are well within the combined uncertainties of the two sensors used to develop the model. The systematic difference (or the accuracy) between the model and satellite measurements is within 3%. Part of the remaining difference is primarily attributed to the real calibration differences between Terra MODIS, EO-1 Hyperion and various sensors under study. It can be seen that the random uncertainties (or precision), shown in Figure 17 are generally better than 2%. Similar work performed by Govaerts *et al.* over Libya 4 showed mean accuracy of 3% when his model was validated with different satellite sensors using three-year observations from 2006 to 2009 [9]. However their approach was based on using solar irradiance as forcing function coupled with a BRDF model and a radiative transfer atmospheric model. Thus the comparison between these two approaches shows that it is possible to develop a PICS-based calibration model with a mean accuracy of 3%. However, his model only extended to SWIR-1 band, whereas the work presented in this article extends up to SWIR-2 band (2,395 nm).

It is interesting to note that both systematic and random does not vary smoothly as a function of wavelength. A portion of this is primarily driven by atmospheric changes as the spectral bandpass differences between Terra MODIS and other sensors are large enough to respond differently to atmospheric conditions at the time of overpass. The empirical atmospheric model did account for the residual seasonal variations in the satellite datasets, but this model is too simple to account for the complex atmospheric phenomenon. Similarly, the empirical BRDF model provided a limiting BRDF samples as the solar zenith angles and the view zenith angle ranges were limited since the orbital conditions of the satellite were fixed. Both the precision and accuracy of the model shown in Figures 16 and 17 can be improved by using the first principles approach, which would use the sun as a solar forcing function rather than using a single sensor as a calibrated radiometer, a surface BRDF model based on the physical properties of the surface and a full up atmospheric transfer model using climatological data. Data from climatological databases such as Aerosol Robotic Network (AERONET) and metrological observation from various National Oceanic and Atmospheric Administration (NOAA) can be used to develop atmospheric model.

4. Summary and Conclusions

PICS have been widely used for monitoring temporal stability and cross calibration of optical sensors, but only few have explored the possibility of using PICS to develop absolute calibration model. This paper makes a strong case for the use of these PICS for absolute calibration model development. This article reported an empirical calibration using Libya 4 PICS where Terra MODIS as a reference radiometer, EO-1 Hyperion to derive spectral information of the target. The model was validated for different satellite sensors such as ETM+, Aqua MODIS, MERIS, Landsat 8 OLI and UK-2 DMC, *etc.* Results showed that the model could predict the satellite measurements with a 3% systematic error and the random uncertainties were generally within 2% across the spectrum for visible to SWIR regions. While the systematic uncertainties were probably driven by the real calibration differences between Terra MODIS and other sensors, the random uncertainties were driven by the atmospheric conditions at the time of overpass. The results from this paper clearly demonstrate the

potential of using PICS for absolute radiometric calibration and inter-calibration among satellite sensors, with particular application to moderate or coarse resolution sensors with viewing angles of up to 20 degrees.

However, the major drawback of the study is that it only used a single sensor as the calibration standard. Also, the model in its current form is restricted to limited viewing geometries of ±20 degrees, beyond which the atmospheric scattering, such as Rayleigh scattering, increases to values which are not accounted for by the simple empirical model. An improvement can be envisioned as a first principles method using the sun as a calibrated source, a full atmospheric model developed through meteorological observations and climatological data, and a full-surface BRDF model developed using the physical properties of sand. Development of a physical model will take time, as thorough understanding of surface properties, surface spectra and the atmosphere over the site is required. However, development of these PICS-based models can lead to an independent, reliable, less expensive and more repeatable radiometric calibration with accuracies of 2% or better.

Acknowledgement

The authors thank David Aaron Larry Leigh and Ameya Vaidya from South Dakota State University (SDSU) for providing useful insights into the work and also numerous other team members from USGS EROS, MCST team, DMCii for their help with Landsat, Hyperion and DMC data that are basis of this work. Finally the authors gratefully acknowledge all the reviewers for improving the manuscript.

Author Contributions

Nischal Mishra and Dennis Helder are members of Digital Image Processing Laboratory South Dakota State University. Bulk of the work presented in this research work, including the writing of the paper was performed by Nischal Mishra. Dennis Helder was his supervisor, mentoring him in the key concepts such as BRDF and atmospheric models to develop an absolute calibration model and making major edits in various sections of the paper. Jack Xiong, Amit Angal and Jason Choi are members of MODIS Characterization Support team. They are responsible for generating the Terra and Aqua MODIS datasets which has been used to generate and validate the proposed absolute calibration model. They have also provided the technical guidance to MODIS calibration and their regular guidance on the concept of the work and reviews on various sections of the paper is important part of this joint endeavor.

Conflicts of Interest

The authors declare no conflict of interest.

References

1. Cosnefroy, H.; Leroy, M.; Briottet, X. Selection and characterization of Saharan and Arabian desert sites for the calibration of optical satellite sensors. *Remote Sens. Environ.* **1996**, *58*, 101–114.

2. Chander, G.; Xiong, X.X.; Choi, T.Y.; Angal, A. Monitoring on-orbit calibration stability of the Terra MODIS and Landsat 7 ETM+ sensors using pseudo-invariant test sites. *Remote Sens. Environ.* **2010**, *114*, 925–939.
3. Rao, C.R.; Chen, J. Revised post-launch calibration of the visible and near-infrared channels of the Advanced Very High Resolution Radiometer (AVHRR) on the NOAA-14 spacecraft. *Int. J. Remote Sens.* **1999**, *20*, 3485–3491.
4. Heidinger, A.K.; Cao, C.; Sullivan, J.T. Using Moderate Resolution Imaging Spectrometer (MODIS) to calibrate advanced very high resolution radiometer reflectance channels. *J. Geophys. Res.* **2002**, doi:10.1029/2001JD002035.
5. Smith, D.L.; Mutlow, C.T.; Rao, C.R.N. Calibration monitoring of the visible and near-infrared channels of the Along-Track Scanning Radiometer-2 by use of stable terrestrial sites. *Appl. Opt.* **2002**, *41*, 515–523.
6. Chander, G.; Mishra, N.; Helder, D.L.; Aaron, D.; Angal, A.; Choi, T.; Xiong, X.; Doelling, D. Applications of spectral band adjustment factors (SBAF) for cross-calibration. *IEEE Trans. Geosci. Remote Sens.* **2013**, *51*, 1267–1281.
7. Govaerts, Y.M.; Clerici, M.; Clerbaux, N. Operational calibration of the Meteosat radiometer VIS band. *IEEE Trans. Geosci. Remote Sens.* **2004**, *42*, 1900–1914.
8. Govaerts, Y.M.; Clerici, M. Evaluation of radiative transfer simulation over bright desert calibration sites. *IEEE Trans. Geosci. Remote Sens.* **2004**, *42*, 176–187.
9. Govaerts, Y.M.; Sterckx, S.; Adriaensen, S. Optical Sensor Calibration Using Simulated Radiances over Desert Sites. In Proceedings of the 2012 IEEE International Geoscience and Remote Sensing Symposium (IGARSS), Munich, Germany, 22–27 July 2012.
10. Bhatt, R.; Doelling, D.R.; Morstad, D.; Scarino, B.R.; Gopalan, A. Desert-based absolute calibration of successive geostationary visible sensors using a daily exoatmospheric radiance model. *IEEE Trans. Geosci. Remote Sens.* **2013**, doi:10.1109/TGRS.2013.2274594.
11. Helder, D.; Thome, K.J.; Mishra, N.; Chander, G.; Xiong, X.; Angal, A.; Choi, T. Absolute radiometric calibration of Landsat using a pseudo invariant calibration site. *IEEE Trans. Geosci. Remote Sens.* **2013**, *51*, 1360–1369.
12. Angal, A.; Xiong, X.X.; Choi, T.; Chander, G.; Mishra, N.; Helder, D.L. Impact of Terra MODIS Collection 6 on long-term trending comparisons with Landsat 7 ETM+ reflective solar bands. *Remote Sens. Lett.* **2013**, *4*, 873–881.
13. Teillet, P.M.; Barsi, J.A.; Chander, G.; Thome, K.J. Prime candidate earth targets for the post-launch radiometric calibration of space-based optical imaging instruments. *Proc. SPIE* **2007**, doi:10.1117/12.733156.
14. Morstad, D.L.; Helder, D.L. Use of Pseudo-Invariant Sites for Long-Term Sensor Calibration. In Proceedings of the IEEE International Geoscience and Remote Sensing Symposium, Boston, MA, USA, 7–11 July 2008.
15. Helder, D.L.; Basnet, B.; Morstad, D.L. Optimized identification of worldwide radiometric pseudo-invariant calibration sites. *Can. J. Remote Sens.* **2010**, *36*, 527–539.

16. Chander, G.; Christopherson, J.B.; Stensaas, G.L.; Teillet, P.M. Online Catalogue of World-Wide Test Sites for the Post-Launch Characterization and Calibration of Optical Sensors. In Proceedings of the International Astronautical Federation—58th International Astronautical Congress, Hyderabad, India, 24–28 September 2007.
17. Barsi, J.A.; Markham, B.; Helder, D.L. In Flight Calibration of Optical Satellite Sensors Using Pseudo Invariant Calibration Sites. In Proceedings of the 2012 IEEE International Geoscience and Remote Sensing Symposium, IGARSS '12, Munich, Germany, 22–27 July 2012.
18. Choi, T.J.; Xiong, X.X.; Angal, A.; Chander, G. Spectral stability of the Libya 4 site using EO-1 Hyperion. *Proc. SPIE* **2013**, doi:10.1117/12.2016644.
19. Lucht, W.; Schaaf, C.B.; Strahler, A.H. An algorithm for the retrieval of albedo from space using semiempirical BRDF models. *IEEE Trans. Geosci. Remote Sens.* **2000**, *38*, 977–998.
20. Roujean, J.L.; Leroy, M.; Deschamps, P.Y. A bidirectional reflectance model of the earth's surface for the correction of remote sensing data. *J. Geophys. Res.: Atmos.* **1992**, *97*, 20455–20468.
21. Snyder, W.C.; Zhang, Z. BRDF models to predict spectral reflectance and emissivity in the thermal infrared. *IEEE Trans. Geosci. Remote Sens.* **1998**, *36*, 214–225.
22. Lacherade, S.; Fougnie, B.; Henry, P.; Gamet, P. Cross calibration over desert sites: Description, methodology, and operational implementation. *IEEE Trans. Geosci. Remote Sens.* **2013**, *51*, 1098–1113.
23. Lawrence, A.; Bernstein, S.; Robertson, D.C. *MODTRAN: A Moderate Resolution Model for LOWTRAN*; No. SSI-TR-124; Spectal Science Inc.: Burlington, MA, USA, 1987.
24. Vermote, E.F.; Tanré, D.; Deuze, J.L.; Herman, M.; Morcette, J.J. Second simulation of the satellite signal in the solar spectrum, 6S: An overview. *IEEE Trans. Geosci. Remote Sens.* **1997**, *35*, 675–686.